

Supporting Information

Halogen-Substituted Phenazine Cores Reduce Energy Losses and Optimize Carrier Dynamics in Tethered Acceptors for 19.8% Efficient and Stable Polymer Solar Cells

Liang Zeng,^a Rong Hu^a, Ming Zhang,^a Seunglok lee^b, ShiXin Meng^a, QingYuan Wang^a, Qi Chen^a,
Lingwei Xue^c, Changduk Yang^b, Zhi-Guo Zhang^{*a}

^a State Key Laboratory of Chemical Resource Engineering, Beijing Advanced Innovation Center for Soft Matter Science and Engineering, Beijing University of Chemical Technology, Beijing 100029, China.

^b Department of Energy Engineering School of Energy and Chemical Engineering Low Dimensional Carbon Materials Center Ulsan National Institute of Science and Technology (UNIST) Ulsan 689-798, South Korea.

^c School of Chemical and Environmental Engineering, Pingdingshan University, Pingdingshan Henan 467000, China

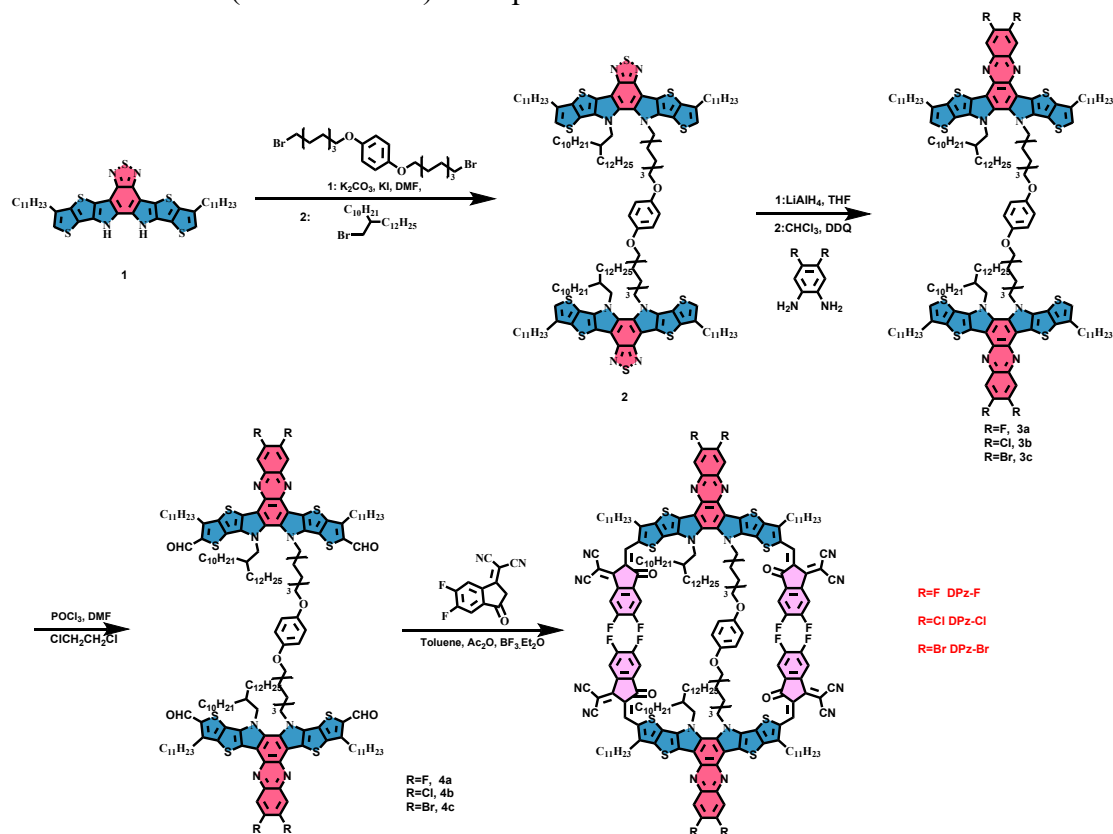
E-mail: zgzhangwhu@iccas.ac.cn (Z.G. Zhang)

Contents

- 1 Materials and Synthesis**
- 2 Fabrication and characterization**
- 3 Supplementary Tables**
- 4 Supplementary Figures**

1. Materials and Synthesis

Materials: The reaction progress was monitored using a thin-layer chromatography (glass backed, extra hard layer, 60 Å, 250 µm thickness, F254 indicator). All chemicals were obtained from commercially available sources and used without further purification. Solvents are used as received. All procedures were carried out under open atmosphere with no precautions taken to exclude ambient moisture. PM6 (used in device) were purchased from Solarmer Materials.



Scheme S1. The synthetic routes of DPz-F, DPz-Cl and DPz-Br

Synthetic Procedures

Synthesis of compound 2:

Compound 1 (1.54 g, 2 mmol), K₂CO₃ (2.20 g, 16 mmol), KI (664 mg, 4 mmol), 1,4-bis((8-bromooctyl)oxy)benzene (442 mg, 0.90 mmol) were added to a 100 mL two-necked, round-bottomed flask with DMF (60 mL) as the solvent. Argon was replaced three times to remove air from the reaction flask. The reaction system was transferred to an oil bath at 80 °C for 24 h. 2-Ethylhexyl bromide (3.34 g, 8 mmol) was added to the reaction system and the mixture was stirred for an additional 12 hours. After the reaction system was cooled to room temperature, it was extracted three times (30 mL×3) with dichloromethane. The organic phase was dried over anhydrous MgSO₄, filtered and subsequently depressurized to remove excess organic solvent. The crude product was eluted with a solvent mixture of PE:DCM (V/V= 3:1) as eluent and separated by

silica gel column chromatography, and the relevant products were collected and vacuum dried to give 1.40 g of yellow solid in about 56.6% yield. ^1H NMR (400 MHz, CDCl_3) δ 7.02 (s, 4H), 6.76 (s, 4H), 4.63 (dd, $J = 18.5, 7.5$ Hz, 8H), 3.77 (t, $J = 6.5$ Hz, 4H), 2.83 (t, $J = 7.6$ Hz, 8H), 2.18 - 2.08 (m, 2H), 1.94 - 1.84 (m, 12H), 1.65 - 1.58 (m, 4H), 1.52 - 0.67 (m, 184H).

Synthesis of compound 3a:

In a 100 mL single-necked round-bottomed flask, compound 2 (1.40 g, 0.56 mmol) and 50 mL of ultra-dry THF were added sequentially and stirred in an ice-water bath for 20 min. 12 ml of THF solution of lithium aluminium hydride (1 mol/L) was added dropwise to the reaction system, and the reaction was continued for 1 h in an ice-water bath, and then finally transferred to an 80 °C oil bath for 10 h. After the reaction system was cooled to room temperature, the reaction material was added dropwise to ice water and extracted with dichloromethane three times (30 mL \times 3). After the reaction system was cooled to room temperature, the reaction product was slowly added dropwise into ice water and extracted with dichloromethane three times (30 mL \times 3). The organic phase was dried by anhydrous MgSO_4 , filtered, and the filtrate was depressurized to remove excess organic solvent, and the crude diamine product was directly dissolved with 15 mL of trichloromethane. Then 3-dichloro-5, 6-dicyano-1, 4-benzoquinone (DDQ, 285 mg, 1.26 mmol, 2.0 eq.) and 4,5-difluorobenzene-1,2-diamine (360 mg, 3.14 mmol) were added sequentially to the solution and the reaction was left to react for 6 h at room temperature. At the end of the reaction, the reaction was poured into a dispensing funnel containing 150 mL and extracted three times with dichloromethane (50 mL \times 3). The organic phase was dried over anhydrous MgSO_4 , filtered and subsequently depressurized to remove excess organic solvent. The crude product was eluted with a solvent mixture of PE:DCM (V/V= 1:1), separated by silica gel column chromatography, and the relevant products were collected and dried under vacuum to give 1.0 g of yellow solid in about 71% yield. ^1H NMR (400 MHz, CDCl_3) δ 8.15 (t, $J = 9.6$ Hz, 4H), 7.03 (d, $J = 4.6$ Hz, 4H), 6.73 (s, 4H), 4.69 (t, $J = 7.4$ Hz, 4H), 4.64 (d, $J = 7.8$ Hz, 4H), 3.76 (t, $J = 6.5$ Hz, 4H), 2.87 (t, $J = 7.7$ Hz, 8H), 2.24 - 2.13 (m, 2H), 2.08 - 1.96 (m, 4H), 1.95 - 1.85 (m, 8H), 1.66 - 1.55 (m, 8H), 1.55 - 0.75 (m, 174H), 0.69 (d, $J = 6.9$ Hz, 6H).

Compound 3b: The synthetic method was similar to **Compound 3a**, which was a red solid (yield=65%). ^1H NMR (400 MHz, CDCl_3) δ 8.53 (s, 4H), 7.02 (d, $J = 7.7$ Hz, 4H), 6.71 (s, 4H), 4.66 (t, $J = 7.3$ Hz, 4H), 4.61 (d, $J = 7.7$ Hz, 4H), 3.75 (t, $J = 6.5$ Hz, 4H), 2.86 (t, $J = 7.7$ Hz, 8H), 2.23 - 2.13 (m, 2H), 2.09 - 1.98 (m, 4H), 1.96 - 1.85 (m, 8H), 1.65 - 1.56 (m, 8H), 1.56 - 0.75 (m, 174H), 0.67 (t, $J = 7.1$ Hz, 6H).

Compound 3c: The synthetic method was similar to **Compound 3a**, which was a red solid (yield=65%). ^1H NMR (400 MHz, CDCl_3) δ 8.70 (s, 4H), 7.02 (d, $J = 8.7$ Hz, 4H), 6.70 (s, 4H), 4.66 (t, $J = 7.3$ Hz, 4H), 4.60 (d, $J = 7.7$ Hz, 4H), 3.75 (t, $J = 6.5$ Hz, 4H), 2.85 (t, $J = 7.4$ Hz, 8H), 2.24 -

2.14 (m, 2H), 2.04 (d, $J = 5.3$ Hz, 4H), 1.94 - 1.84 (m, 8H), 1.66 - 1.55 (m, 8H), 1.52 - 0.76 (m, 174H), 0.67 (t, $J = 7.1$ Hz, 6H).

Synthesis of compound 4a:

To DMF (1 ml) in a two-necked flask, phosphorus oxychloride (4.5mmol) was added by injector, and the mixture was stirred for 30 min at 0 °C under argon atmosphere. The mixture was then transferred to a solution of **compound 3a** (409 mg, 0.2 mmol) and 50 ml dichloroethane in another two-necked flask, heated to 90 °C and refluxed overnight under argon atmosphere. The mixture was poured into water to quench the reaction and extracted by DCM. The organic layer was washed with saturated aqueous solution of sodium carbonate (200 ml) several times and dried with MgSO₄. After concentration under reduced pressure, flash column chromatography with DCM as the eluents to afford the final product as a orange solid(359 mg, 83.2%).¹H NMR (400 MHz, CDCl₃) δ 10.16 (s, 4H), 8.13 (td, $J = 9.1, 2.2$ Hz, 4H), 6.70 (s, 4H), 4.75 (t, $J = 7.4$ Hz, 4H), 4.67 (d, $J = 7.9$ Hz, 4H), 3.76 (t, $J = 6.5$ Hz, 4H), 3.23 (t, $J = 7.7$ Hz, 8H), 2.19 - 2.10 (m, 2H), 2.00 (m, 12H), 1.66 - 0.75 (m, 182H), 0.67 (t, $J = 7.0$ Hz, 6H).

Compound 4b: The synthetic method was similar to **Compound 4a**, which was a red solid (yield=65%).¹H NMR (Compound 4b, 400 MHz, CDCl₃) δ 10.15 (d, $J = 7.9$ Hz, 4H), 8.36 (d, $J = 14.3$ Hz, 4H), 6.59 (s, 4H), 4.80 - 4.72 (m, 4H), 4.63 (d, $J = 7.8$ Hz, 4H), 3.74 (t, $J = 6.4$ Hz, 4H), 3.19 (dd, $J = 14.9, 7.2$ Hz, 8H), 2.13 (d, $J = 4.6$ Hz, 6H), 2.03 - 1.87 (m, 8H), 1.66 - 1.60 (m, 4H), 1.59 - 0.57 (m, 184H).

Compound 4c: The synthetic method was similar to **Compound 4a**, which was a red solid (yield=65%).¹H NMR (400 MHz, CDCl₃) δ 10.15 (d, $J = 9.9$ Hz, 4H), 8.47 (d, $J = 17.2$ Hz, 4H), 6.49 (s, 4H), 4.78 (t, $J = 7.4$ Hz, 4H), 4.65 (d, $J = 7.8$ Hz, 4H), 3.70 (t, $J = 6.1$ Hz, 4H), 3.16 (dd, $J = 15.7, 8.0$ Hz, 6H), 2.24 - 2.12 (m, 6H), 2.01 - 1.86 (m, 8H), 1.66 - 1.59 (m, 4H), 1.56 - 0.83 (m, 174H), 0.76 (t, $J = 7.2$ Hz, 6H), 0.67 (t, $J = 6.9$ Hz, 6H).

Synthesis of compound DBz-F

Compound 5a (216 mg, 0.10 mmol) and 2-(5,6-difluoro-3-oxo-2,3-dihydro- 1H-inden-1-ylidene) malononitrile (92.0 mg, 0.40 mmol) were dissolved in anhydrous toluene (10 ml) under argon atmosphere. Boron trifluoride ether (20 μ l) and acetic anhydride (0.1 ml) were added by injector. After stirring at room temperature for 1 hour, the mixture was poured into methanol (50 ml) and filtered. The residue was purified by short flash column chromatography on a silica gel column using PE:DCM=1:2 (V:V) as eluent to afford a black solid(295 mg, 98.2%).

¹H NMR (DPz-F, 400 MHz, CDCl₃) δ 8.67 (s, 2H), 8.56 (s, 2H), 8.37 - 8.08 (m, 8H), 7.59 (t, $J = 6.9$ Hz, 4H), 6.62 (s, 4H), 4.95 - 4.62 (m, 8H), 3.89 (t, $J = 6.5$ Hz, 4H), 3.02 (t, $J = 7.7$ Hz, 8H), 2.58 - 2.40 (m, 4H), 2.19 - 2.06 (m, 2H), 1.98 - 1.63 (m, 26H), 1.53 - 0.63 (m, 173H).

^{13}C NMR (DPz-F, 100 MHz, CDCl_3) δ 185.79, 158.83, 157.62, 155.29, 153.71, 153.01, 152.73, 152.55, 146.18, 139.24, 137.61, 137.34, 136.81, 136.21, 134.18, 134.13, 133.99, 133.60, 132.57, 132.34, 131.48, 130.86, 122.36, 120.80, 119.32, 118.53, 118.05, 115.07, 114.54, 114.43, 114.28, 111.81, 99.95, 68.30, 55.11, 51.58, 39.67, 31.95, 31.89, 31.85, 31.00, 29.98, 29.73, 29.63, 29.63, 29.52, 29.39, 29.34, 29.29, 27.11, 26.08, 22.72, 22.70, 22.66, 22.62, 14.12, 14.05.

MS (MALDI-TOF) of DPz-F m/z: $[\text{M}+\text{H}]^+$ calcd for $\text{C}_{214}\text{H}_{242}\text{F}_{12}\text{N}_{16}\text{O}_6\text{S}_8$, 3615.67, found in: 3615.67.

Compound DPz-Cl: The synthetic method was similar to **compound DBz-F**, which was a black solid (304 mg, 98.2%).

^1H NMR (DPz-Cl, 400 MHz, CDCl_3) δ 8.71 (s, 4H), 8.26 - 8.15 (m, 8H), 7.70 - 7.56 (d, 4H), 6.42 (s, 4H), 4.96 - 4.64 (m, 8H), 3.75 (t, $J = 6.5$ Hz, 4H), 3.01 (m, $J = 7.7$ Hz, 8H), 2.53 - 2.34 (m, 4H), 2.22 - 2.09 (m, 3H), 1.89 - 1.56 (m, 26H), 1.49 - 0.67 (m, 164H).

^{13}C NMR (DPz-Cl, 100 MHz, CDCl_3) 185.77, 172.17, 159.92, 157.59, 155.63, 153.53, 152.91, 148.09, 147.50, 146.15, 143.82, 139.86, 138.07, 136.84, 136.35, 134.22, 132.93, 131.22, 129.17, 129.17, 124.76, 119.37, 118.05, 137.30, 116.72, 114.81, 114.62, 114.25, 112.30, 112.11, 110.18, 68.08, 55.25, 49.74, 39.78, 31.95, 31.90, 31.86, 31.18, 30.10, 30.08, 29.77, 29.72, 29.68, 29.65, 29.60, 29.41, 29.35, 29.32, 29.22, 25.82, 22.71, 22.66, 22.63, 14.13, 14.08, 14.06.

MS (MALDI-TOF) of DPQx-F m/z: $[\text{M}+\text{H}]^+$ calcd for $\text{C}_{214}\text{H}_{242}\text{Cl}_4\text{F}_8\text{N}_{16}\text{O}_6\text{S}_8$, 3679.55, found in: 3679.59.

Compound DPz-Br: The synthetic method was similar to **compound DBz-F**, which was a black solid (304 mg, 98.2%).

^1H NMR (DPz-Br, 400 MHz, CDCl_3) δ 8.74 (s, 4H), 8.53 - 5.13 (m, 8H), 7.67 (d, $J = 7.4$ Hz, 4H), 6.33 (s, 4H), 5.02 - 4.63 (m, 8H), 3.70 (t, $J = 6.5$ Hz, 4H), 3.01 (t, $J = 7.7$ Hz, 8H), 2.52 - 2.34 (m, 4H), 2.27 - 2.13 (m, 2H), 1.92 - 1.56 (m, 26H), 1.50 - 0.64 (m, 163H).

^{13}C NMR (DPz-Br, 100 MHz, CDCl_3) 185.90, 181.59, 177.28, 165.31, 157.61, 155.34, 153.41, 152.85, 152.76, 146.18, 140.14, 136.98, 136.22, 135.53, 134.20, 133.15, 132.93, 132.49, 129.01, 125.86, 122.37, 119.30, 118.35, 118.12, 114.75, 144.22, 112.18, 110.31, 67.50, 57.87, 55.35, 53.38, 51.69, 39.82, 37.06, 31.95, 31.90, 31.87, 31.23, 30.15, 29.97, 29.78, 29.73, 29.68, 29.65, 29.41, 29.35, 29.33, 22.71, 22.67, 22.64, 14.13, 14.08, 14.07.

MS (MALDI-TOF) of DPz-Br m/z: $[\text{M}+\text{H}]^+$ calcd for $\text{C}_{214}\text{H}_{242}\text{Br}_4\text{F}_8\text{N}_{16}\text{O}_6\text{S}_8$, 3855.35, found in: 3862.36.

2. Fabrication and characterization

^1H NMR and ^{13}C NMR: ^1H NMR, ^{13}C NMR and ^1H - ^1H NOESY NMR spectra were recorded on Bruker AVANCE 400 MHz NMR spectrometer with CDCl_3 as a solvent.

MALDI-TOF: MALDI-TOF mass spectrometry experiments were performed on an autoflex III instrument (Bruker Daltonics, Inc.).

TGA: TGA was measured on HTG-1 Thermogravimetric Analyzer (Beijing Hengjiu Experiment Equipment Co. Ltd.) with a heating rate of 10 °C min⁻¹ under a nitrogen flow rate of 100 mL min⁻¹.

UV-visible absorption: The UV-vis absorption spectra were measured by Hitachi U-2910 UV-vis spectrophotometer. In the case of solution absorbance measurement, the dilute solution of acceptors in chloroform (1×10^{-5} M) was prepared to be measured. Besides, the thin film samples were prepared by spin-coating (3000 rpm) acceptors' chloroform solutions (10 mg ml⁻¹) on quartz plates. The as-cast thin films all performed a thickness ranging from 50 nm to 80 nm, which were recorded on Bruker DEKTAK XT step profiler.

Cyclic voltammetry: Cyclic voltammetry was conducted on a Zahner IM6e electrochemical workstation using sample films coated on glassy carbon as the working electrode, Pt wire as the counter electrode, and Ag/AgCl as the reference electrode, in a 0.1 M tetrabutylammonium hexafluorophosphate (Bu₄NPF₆) acetonitrile solution and ferrocene/ferrocenium (Fc/Fc⁺) couple was used as an internal reference.

DFT calculation : The optimization and the singlet point energy of simplify structures including DPz-F, DPz-Cl and DPz-Br were performed at the B3LYP/ 6-31 G (d,p) level using Gaussian 09 package. Multiwfn is used for data analysis and processing

Device fabrication and characterization of the PSCs: The PSCs were fabricated with a structure of ITO/2PACz/active layer/PDINN/ Ag. The ITO glass was cleaned by sequential ultrasonic treatment in water, deionized water, acetone and isopropanol, and then treated in an ultraviolet ozone cleaner (Ultraviolet Ozone Cleaner, Northern Scientific Inc, USA) for 10 min. The 2PACz aqueous solution was filtered through a 0.45 mm filter and then spin-coated on pre-cleaned ITO-coated glass at 4000 rpm for 30 s. Subsequently, A blend solution of D18 donor and TSMA was prepared by dissolving the materials in chloroform with a total concentration of 13 mg/ml (D:A=1:1.3), and 0.6% (V/V) 1-chloroanthracene as additive, and then was spin-coated at 5300 rpm onto the 2PACz layer. Then methanol solution of PDINN at a concentration of 1.0 mg mL⁻¹ was deposited on the active layer at 3000 rpm for 30 s to afford a cathode buffer layer. Finally, the metal cathode Ag was thermal evaporated under a mask at a base pressure of approximately 10⁻⁵ Pa. The photovoltaic area of the device is 6 mm². The current-voltage (J-V) curves of PSCs

were measured in a high-purity nitrogenfilled glove box using a Keithley B2901A source meter. AM 1.5 G irradiation at 100 mW cm⁻² is provided by simulator (SS-F5-3A, Enlitech, AAA grade, 70× 70 mm² photobeam size) in glove box, which was calibrated by standard silicon solar cells. The current density-voltage (*J*-*V*) characteristic were measured by using the solar simulator (SS-F5-3A, Enlitech, Taiwan) along with AM 1.5 G (100 mW/cm²) with step 0.02 V and delay time 10 ms. The external quantum efficiency (EQE) spectra of PSCs were measured in air conditions by a solar cell spectral response measurement system (QER3011, Enlitech).

SCLC mobility measurement (SCLC): The structure of electron-only devices is ITO/ZnO/active layer/PDINN/Ag and the structure of hole-only devices is ITO/PEDOT:PSS/active layer/MoO₃/Ag. In these device structures, the same fabrication conditions as OSCs are used to form the active layer films. The charge mobilities are generally described by the Mott-Gurney equation

$$J = \frac{9}{8} \epsilon_0 \epsilon_r \mu \frac{V}{d^3}$$

where *J* is the current, μ is the zero-filed mobility, $\epsilon_0 = 8.85 \times 10^{-12}$ F/m, is the permittivity of free space and ϵ_r is the relative permittivity of the material (This part assumes the ϵ_r to be 3 for each active layer) . *V* is the effective voltage, and *d* is the thickness of the organic layer, measured by a profilometer. The effective voltage can be obtained by subtracting the built-in voltage (*V*_{bi}) and the voltage drop (*V*_s) from the substrate's series resistance from the applied voltage (*V*_{appl}), $V = V_{\text{appl}} - V_{\text{bi}} - V_{\text{s}}$. The hole and electron mobility can be evaluated from the slope of the *J*^{1/2}-*V* curves.

Estimation of glass-transition temperature:

UV-vis spectroscopy was used to determine the glass transition temperature (*T*_g). The absorption spectra of dimer films were measured with increasing temperatures from 80 to 200 °C. For the preparation of dimer films, we used the same processing conditions (i.e., solvent, concentration, and spin coating speed) as those for the PSC fabrication, to precisely correlate the estimated *T*_g with those in the PSC device. Then, the deviation metric (DMT) of each absorption spectra were calculated, following the method reported by Harald Ade^[6]

$$DMT = \sum_{\lambda_{\min}}^{\lambda_{\max}} [I_{RT}(\lambda) - I_T(\lambda)]^2$$

where λ is the wavelength, λ_{\max} and λ_{\min} are the upper and lower bounds of the optical sweep, respectively, $I_{RT}(\lambda)$ and $I_T(\lambda)$ are the normalized absorption intensities of the as-cast (room

temperature) and annealed films, respectively. Then, the T_g is determined to be the point where the two interpolated lines in low- and high-temperature regions intersect.

Thermal stability :Stability of the PSCs: The PSCs for thermal stability measurement were fabricated with an inverted structure of ITO/ZnO/D18:acceptors/MoO_x/Ag for preventing diffusion of organic cathode interlayer.

The OSCs used for photostability measurement were encapsulated and tested in the air. A multichannel solar cell performance decay test system (PVL-6001M-32A, Suzhou D&R Instruments Co. Ltd.) and continuous white LED light (D&R Light, L-W5300KA-150, Suzhou D&R Instruments Co. Ltd.) were applied. The initial illumination intensity was adjusted to match the J_{sc} measured under standard conditions by AM 1.5G. During the test, the illumination intensity was monitored using a photodiode. Periodic J–V characterization of the devices allowed for the calculation of photovoltaic parameters, including V_{oc} , J_{sc} , FF, and PCE according to the J – V curves.

Encapsulation details:After bonding the silver electrode surface with the glass sheet using UV Curing Adhesive, the adhesive was cured for 120 seconds under a 360 nm UV flashlight.

GIWAXS experiment:The GIWAXS measurement was carried out at the PLS-II 6D U-SAXS beamline of the Pohang Accelerator Laboratory in Korea. The scattering signal was recorded using a 2-D CCD detector (Rayonix SX165). The X-ray light had an energy of 11.564 KeV. The incidence angle of X-rays was adjusted to 0.08°.

TPC & TPV: TPC & TPV tests were conducted on an LST-TPVC transient photo current & voltage measuring instrument (Shanghai Hongpei Technology Co., Ltd).

Contact angle method :

Owen Method for calculating the surface energy. The Owen's method is often used to calculate the surface energy:

$$\gamma_s = \gamma_s^D + \gamma_s^P, \gamma_l = \gamma_l^D + \gamma_l^P$$

where γ_s is composed of the dispersion force γ_s^D and polarity force γ_s^P , γ_l is surface energy of the liquid and consists of a dispersion force γ_l^D and polarity force γ_l^P . We can know the surface energies γ_l^D and γ_l^P of the testing liquid and its contact angle on solid film. And according to the formula:

$$\gamma_l(1 + \cos \theta) = 2 \left(\gamma_s^D \gamma_l^D \right)^{\frac{1}{2}} + 2 \left(\gamma_s^P \gamma_l^P \right)^{\frac{1}{2}}$$

We need two known testing liquids to determine γ_s^D and γ_s^P .

$$\gamma_{l1}(1 + \cos \theta) = 2 \left(\gamma_s^D \gamma_{l1}^D \right)^{\frac{1}{2}} + 2 \left(\gamma_s^P \gamma_{l1}^P \right)^{\frac{1}{2}}$$

$$\gamma_{l2}(1 + \cos \theta) = 2 \left(\gamma_s^D \gamma_{l2}^D \right)^{\frac{1}{2}} + 2 \left(\gamma_s^P \gamma_{l2}^P \right)^{\frac{1}{2}}$$

Finally, γ_s can be determined by.

$$\gamma_s = \gamma_s^D + \gamma_s^P$$

Solubility parameter (δ) can be calculated from the surface tension, $\delta = K\sqrt{\gamma}$. where γ is the surface tension, K is the proportionality constant ($K = 116 \times 103 \text{ m}^{-1/2}$). And Flory-Huggins interaction parameter (χ_{ij}) can be written as a function of two solubility parameters,

$$\chi_{ij} = \kappa(\sqrt{\gamma_i} - \sqrt{\gamma_j})^2 \quad \chi_{D-A} = (\sqrt{\gamma_D} - \sqrt{\gamma_A})^2$$

Quantification for Energy Loss: FTPLS-EQE measurement. FTPLS-EQE was recorded by using a Vertex 70 from Bruker Optics with an external detector option. A low-noise current amplifier (SR570) was employed to amplify the photocurrent generated from the photovoltaic devices with illumination light modulated by the Fourier transform infrared (FTIR) instrument. EQEEL measurement. EQE_{EL} values were achieved from a home-built setup containing a Hamamatsu silicon photodiode 1010B, a Keithley 2400 SourceMeter for supplying voltages and recording the injected current, and a Keithley 485 for measuring the emitted light intensity. EL measurement. EL spectra were measured with an Andor spectrometer (Shamrock sr-303i-B, coupled to a Newton EMCCD Si arrow detector cooled to -60 °C). A Keithley 2400 external current/voltage source meter was connected to prepare solar cells comprising neat or blend films to support an external electric field for EL measurements.

AFM: AFM measurements were performed by using Bruker Nano Inc. From America. All film samples were spin-cast on ITO substrates.

TEM: Transmission electron microscope (TEM) studies were conducted with a FEI Tecnai G2 F20

electron microscopy to investigate the phase distribution of the active layer, and with the scale bar is 200 nm.

3. Supplementary Tables

Table S1. GIWAXS structural parameters of the D18, DPz-F, DPz-Cl, DPz-Br, D18:DPz-F, D18:DPz-Cl and D18:DPz-Br blend films.

	out of plane (010)			in plane (100)		
	location (\AA^{-1})	d-spacing (\AA)	CCL (\AA)	location (\AA^{-1})	d-spacing (\AA)	CCL (\AA)
D18	0.329	18.1	93.6	1.65	3.80	31.4
DPz-F	0.307	20.4	109.0	1.706	3.683	25.4
DPz-Cl	0.302	20.8	105.6	1.704	3.687	26.1
DPz-Br	0.302	20.8	99.8	1.702	3.92	25.8
D18:DPz-F	0.323	19.4	148.4	1.689	3.720	37.3
D18:DPz-Cl	0.323	19.5	137.4	1.687	3.724	38.7
D18:DPz-Br	0.323	19.4	135.9	1.686	3.727	37.8

Table S2. Photovoltaic parameters for 15 individual devices based on D18:DPz-F

Devices	V_{oc} (V)	J_{sc} (mA cm^{-2})	FF (%)	PCE (%)
1	0.903	26.496	82.16	19.65
2	0.904	26.462	81.77	19.56
3	0.902	26.463	81.86	19.54
4	0.903	26.403	81.69	19.48
5	0.906	26.460	81.56	19.55
6	0.902	26.436	81.59	19.45
7	0.903	26.596	82.08	19.71
8	0.902	26.669	81.23	19.54
9	0.903	26.520	81.25	19.45
10	0.904	26.581	82.42	19.80
11	0.902	26.338	81.50	19.36
12	0.904	26.581	81.38	19.55
13	0.904	26.467	82.44	19.72
14	0.904	26.461	82.01	19.62
15	0.905	26.409	81.51	19.49

Table S3. photovoltaic performance data based on reported dimerized acceptors based binary devices.

Donor	Acceptor	V_{oc} (V)	J_{sc} (mA cm ⁻²)	FF%	PCE%	Ref.
PM6	DPz-F	0.904	26.58	82.42	19.80	This Work
	DPz-Cl	0.906	25.35	78.07	17.95	
	DPz-Br	0.907	25.91	78.87	18.50	
	D-TPh	0.946	25.59	78.7	19.05	<i>Angew. Chem. Int. Ed.</i> , 2024, e202411044.
	D-TN	0.230	25.33	78.2	18.42	
	CH8-6	0.891	26.23	77.8	18.2	<i>Energy Environ. Sci.</i> 2024 ,17, 5719-5729
	CH8-7	0.904	24.97	78.3	17.7	
	CH8-T	0.869	25.92	75.4	17.0	
	DC9-HD	0.900	26.2	79.3	18.7	<i>Adv. Energy Mater.</i> 2024, 2404062.
	DYSe-3	0.864	27.5	78.3	18.6	
	CH8-4	0.901	26.68	75.4	18.1	<i>Angew. Chem. Int. Ed.</i> 2025 , e202423562.
	CH8-4A	0.920	24.20	74.5	16.7	
	CH8-4B	0.906	26.09	75.2	17.8	
	CH8-6	0.891	26.23	77.8	18.2	<i>Energy Environ. Sci.</i> 2024 ,17, 5719-5729
	CH8-7	0.904	24.97	78.3	17.7	
	HDY-m-TAT	0.915	23.22	67.8	14.42	<i>Angew. Chem. Int. Ed.</i> , 2024 , 63, e202403139
	FDY-m-TAT	0.911	26.47	74.7	18.07	
	HDY-o-TAT	0.933	23.07	70.7	15.23	
	FDY-o-TAT	0.914	25.14	73.6	16.91	
	B-DL	0.949	18.563	52.11	9.17	<i>Angew. Chem. Int. Ed.</i> 2024 , 63, e202403005.
	BT-DL	0.940	25.523	77.087	18.49	
	DYSe-1	0.885	27.51	76.6	18.56	<i>Adv. Energy Mater.</i> , 2024 , 14, 2400938.
	DYSe-2	0.884	27.45	75.2	18.22	<i>Adv. Energy Mater.</i> , 2023 , 2300301
	CH-D1	0.949	23.90	73.20	16.62	
	CH8-0	0.936	22.61	72.1	15.26	<i>Energy Environ. Sci.</i> , 2023 ,16, 1773-1782
	CH8-1	0.923	24.89	74.2	17.05	
	CH8-2	0.928	24.24	74.9	16.84	
	CH8-3	0.915	24.44	77.0	17.22	<i>Angew. Chem. Int. Ed.</i> , 2023 , e202307962
CH8-4	0.894	26.05	75.5	17.58		
CH8-5	0.902	24.75	75.2	16.79		
DY1	0.87	25.67	73.24	16.46	<i>Adv. Mater.</i> , 2023 , 35, 2206563.	
DY2	0.87	26.60	76.85	17.85		
DY3	0.87	26.20	76.21	17.33		
DYBO	0.968	24.62	75.8	18.08	<i>Joule.</i> , 2023 , 7, 416.	

	DP-BTP	0.96	22.73	69.10	15.08	<i>Angew. Chem. Int. Ed.</i> 2024 , 63, e2023160
	DYT	0.94	24.08	76	17.30	<i>ACS Energy Lett.</i> , 2023 , 8, 1344.
	DYV	0.93	25.64	78	18.60	
	DYTVT	0.95	24.82	74	17.68	
	2BOHD-T	0.946	24.92	75.02	17.68	<i>Nano. Energy.</i> 2023 , 121, 109218
	2BOHD-TC ₄ T	0.980	22.82	73.75	16.50	
	2BOHD-TC ₆ T	0.976	21.89	70.55	15.07	
	TDY- α	0.864	26.9	78.0	18.10	<i>Nat. Commun.</i> , 2023 , 14, 2926.
	TDY- β	0.849	26.1	76.6	17.00	
	Dimer-Qx	0.933	22.57	69.26	14.59	<i>Adv. Mater.</i> 2024 , 36, 2310046
	Dimer-2CF	0.900	26.39	80.03	19.02	
	2-BTP-2F-T	0.911	25.50	78.28	18.19	<i>Adv. Sci.</i> , 2022 , 9, 2202513.
	EV-i	0.897	25.83	76.56	18.27	<i>Angew. Chem. Int. Ed.</i> , 2023 , 62, e202303551.
	EV-o	0.957	6.20	42.13	2.50	
	DIBP3F-Se	0.917	25.92	76.1	18.09	<i>Angew. Chem. Int. Ed.</i> , 2023 , 62, e2023028
	DIBP3F-S	0.901	24.86	72.0	16.11	
	DY-T	0.949	22.57	72.47	15.52	<i>CCS Chem.</i> , 2023 , 5, 2576
	DY-TF	0.945	24.36	72.87	16.77	
	DYF-TF	0.939	25.82	75.30	18.26	
	DYA-I	0.938	25.67	78	18.83	<i>Adv. Energy Mater.</i> , 2023 , 13, 2301283
	DYA-IO	0.948	24.29	76	17.54	
D18	DYA-O	0.961	23.32	73	16.45	
	DBY-2Cl	0.927	20.76	68.76	13.23	<i>Adv. Funct. Mater.</i> 2024 , 2404919.
	DTY-2Cl	0.913	26.20	75.46	18.06	
	2Y-wing	0.850	27.66	75.4	17.73	<i>Angew. Chem. Int. Ed.</i> , 2024 , 63, e202319295.
	2Y-core	0.864	10.58	61.5	5.63	
	2Y-end	0.948	22.39	68.5	14.46	
	DYV	0.915	24.90	75.20	17.38	<i>ACS Appl. Mater. Interfaces.</i> , 2024 , 16, 7317-7326.
	DYFV	0.897	25.50	77.40	17.88	
	GMA-SSS	0.913	27.13	75.35	18.66	<i>Energy Environ. Sci.</i> 2024 , 17, 9144-9153.
	GMA-SSeS	0.917	27.38	77.12	19.37	
	GMA-SeSSe	0.882	27.47	74.99	18.17	
	GMA-SeSeSe	0.865	26.91	70.83	16.49	<i>Adv. Funct. Mater.</i> , 2023 , 2305608
PBQx-	dB TIC- δ V-BO	0.96	20.67	66.06	13.15	
H-TF	dB TIC- γ V-BO	0.91	24.52	76.58	17.14	
	dB TIC- γ V-OD-2Cl	0.87	24.65	74.71	16.04	

Table S4. photovoltaic performance data based on reported TMSA-type dimerization-based binary devices

Active layer	V_{oc} (V)	J_{sc} (mA cm ⁻²)	FF (%)	PCE (%)	Ref
PM6:DY2	0.870	26.60	76.85	17.85	<i>Adv. Mater.</i> 2023, 35 , 2206563
PM6:DY- P2EH	0.905	24.03	78.58	17.09	<i>Adv. Mater.</i> 2024, 36 , 2308606
PM6:BDY- α	0.869	26.09	76.68	17.38	<i>Angew. Chem. Int. Ed.</i> 2024, 63 , e202400590
PM6:TDY- α	0.864	26.9	78.0	18.10	<i>Nat Commun.</i> 2023, 14 , 2926
D18:DY-Cl	0.883	26.72	79.35	18.72	
D18:DY-Br	0.876	26.45	78.10	18.10	
D18:DL-Cl	0.923	24.95	79.45	18.30	<i>Small.</i> 2025, 21, 2411409
D18:DL-Br	0.926	23.54	78.08	17.02	
D18:DPz-F	0.904	26.58	82.42	19.80	
D18:DPz-Cl	0.906	25.35	78.07	17.95	This Work
D18:DPz-Br	0.907	25.91	78.87	18.50	

Table S5. The distributions of total energy loss in solar cells based on the SQ limit theory.

Active Layer	E_{ga} (eV)	V_{oc} (V)	ΔE (eV)	ΔE_1 (eV)	ΔE_2 (eV)	ΔE_3 (eV)	E_U	EQE_{EL} (%)
PM6:DY2	1.430	0.85	0.580	0.26	0.05	0.27		
PM6:DY- P2EH	1.430	0.898	0.532	0.263	0.043	0.226	22.75	0.016
PM6:BDY- α	1.411	0.865	0.546	0.261	0.054	0.231	23.11	0.014
PM6:TDY- α	1.420	0.864	0.556	0.266	0.058	0.232	23.37	0.013
D18:DY-Cl	1.437	0.887	0.550	0.263	0.047	0.240	22.83	0.009
D18:DY-Br	1.441	0.884	0.557	0.262	0.049	0.246	22.97	0.008
D18:DL-Cl	1.498	0.924	0.574	0.266	0.063	0.244	24.14	0.008
D18:DL-Br	1.502	0.919	0.583	0.266	0.066	0.251	24.48	0.006
D18:DY2	1.422	0.884	0.538	0.262	0.046	0.235	22.80	0.013
D18:DPz-F	1.432	0.904	0.528	0.262	0.040	0.226	22.25	0.016
D18:DPz-Cl	1.432	0.906	0.526	0.262	0.042	0.222	22.29	0.017

D18:DPz-Br 1.432 0.907 0.525 0.262 0.044 0.219 22.77 0.018

Table S6. Summary of contact angles (θ), surface tensions (γ), and Flory–Huggins interaction parameters (χ) for D18 and DPz-F, DPz-Cl and DPz-Br films.

Film	Contact angle [°]		γ (mN m ⁻¹)	χ
	Water	Glycerol		
D18	104.8	94.8	21.13	
DPz-F	99.8	91.1	16.73	0.29
DPz-Cl	102.0	92.8	15.07	0.51
DPz-Br	100.2	91.3	15.69	0.40

4. Supplementary figures

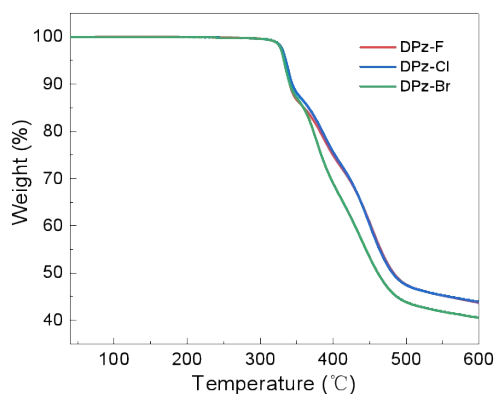


Fig.S1. Thermogravimetric analysis ($10\text{ }^{\circ}\text{C min}^{-1}$) of DPz-F, DPz-Cl and DPz-Br respectively.

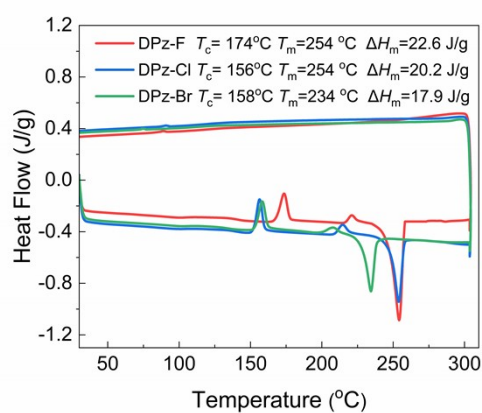


Fig.S2. DSC curves of DPz-F, DPz-Cl and DPz-Br respectively.

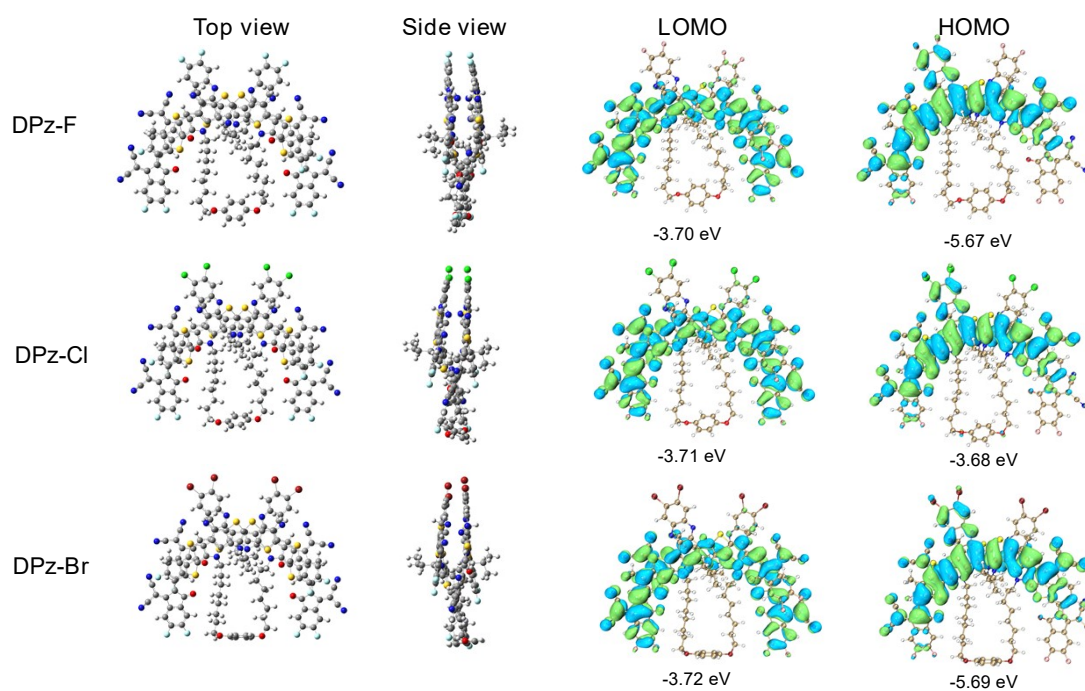


Fig.S3. Optimized geometries, energy levels, and chemical geometry of the molecular models for

DPz-F, DPz-Cl and DBz-Br.

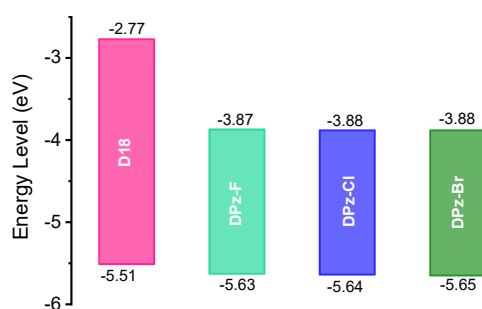


Fig.S4. The energy levels of D18, DPz-F, DPz-Cl and DBz-Br.

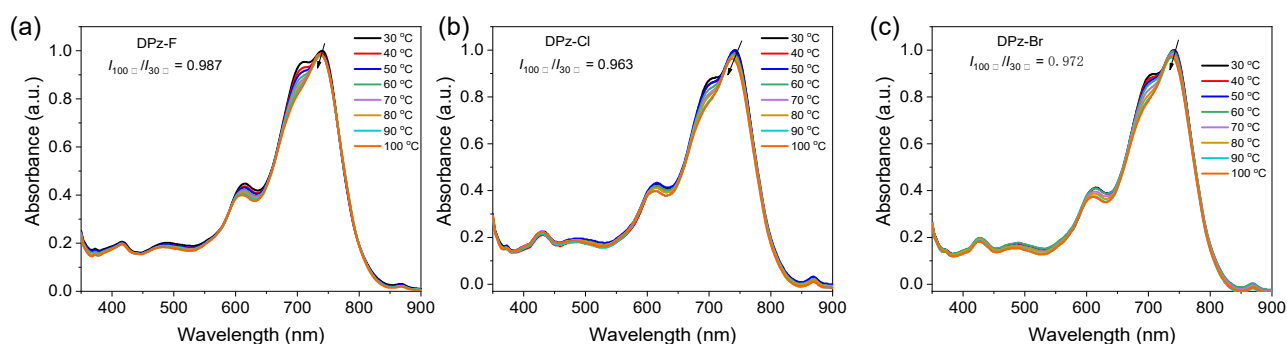


Fig. S5. UV-vis absorption spectra of DPz-F , DPz-Cl and DPz-Br in chlorobenzene solution as a function of temperature.

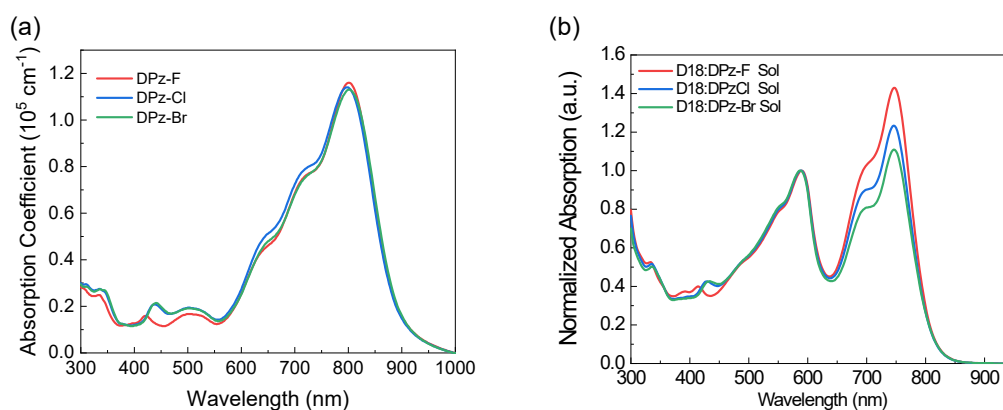


Fig.S6. (a) Absorption coefficient of the DPz-F, DPz-Cl and DBz-Br Film. (b) Absorption spectra of D18:DPz-F, D18:DPz-Cl and D18:DPz-Br in chloroform solution.

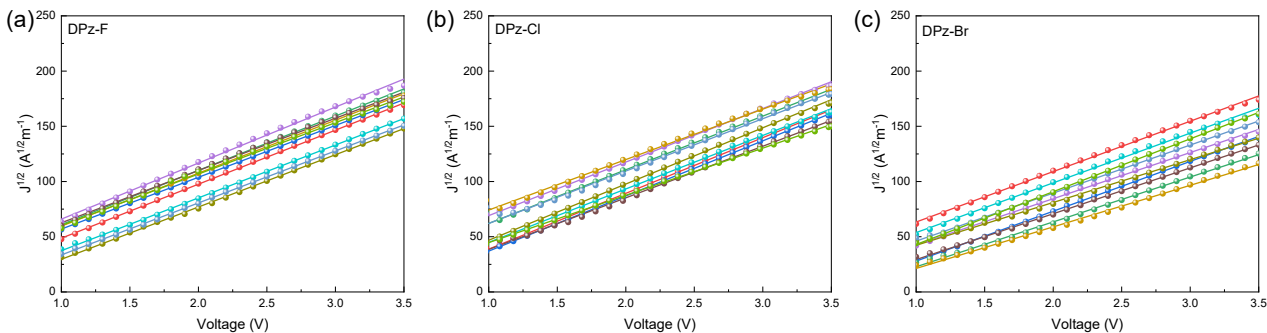


Fig. S7. $J^{1/2}$ - V curves of electron-only devices based on the DPz-F , DPz-Cl and DPz-Br neat films.

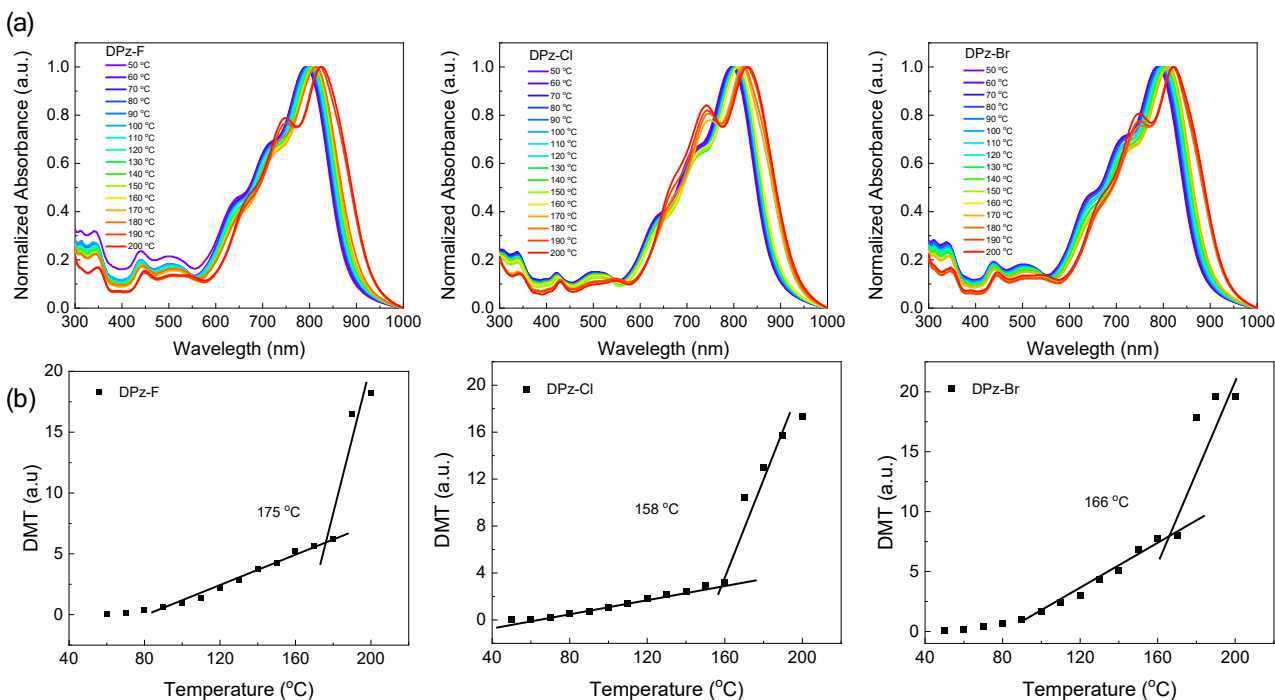


Fig. S8. (a) Normalized absorption spectra of DPz-F, DPz-Cl and DPz-Br thin films from 50 °C to 200 °C. (b): T_g of TSMAs evaluated from DMT data.

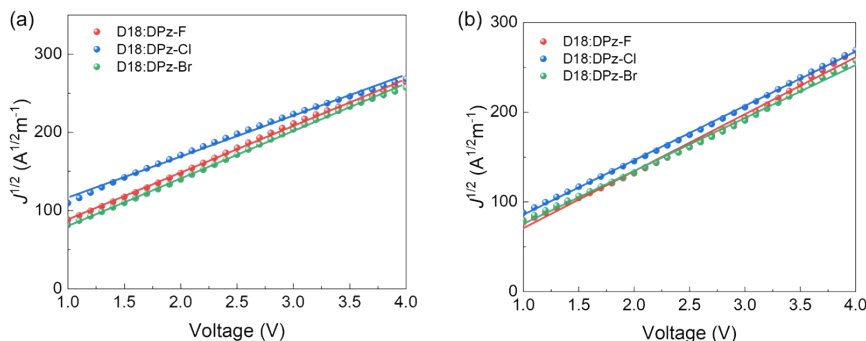


Fig.S9. SCLC fits electron-only and hole-only devices based on the D18:DPz-F, D18:DPz-Cl and D18:DPz-Br blend films

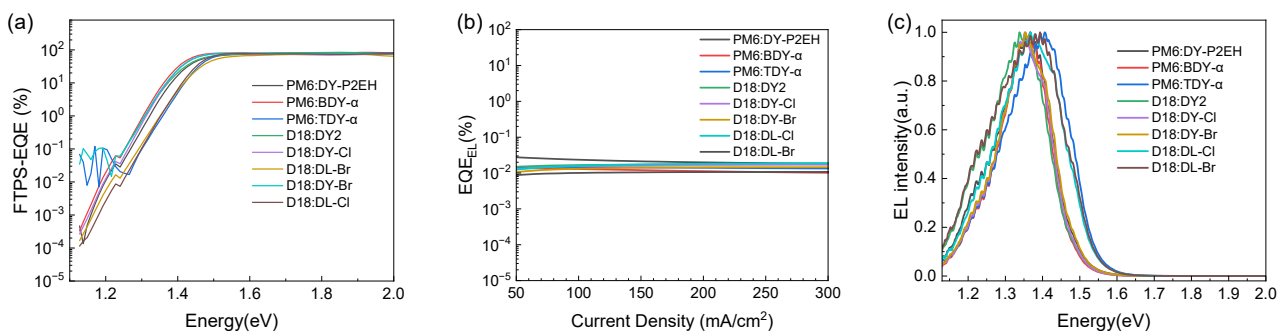


Fig. S10. (a) FTPS-EQE Spectrum; (b) EQE_{EL} curves and (c) Normalized EL spectra of reported devices with TMSA-type dimers

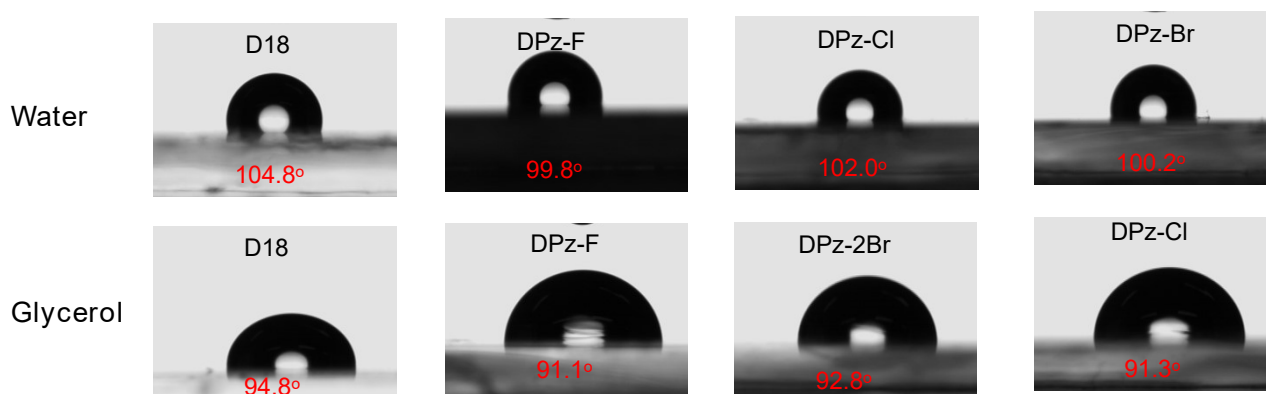


Fig. S11. Contact angle (CA) images, surface tension (γ) of pure donor D18 and acceptors.

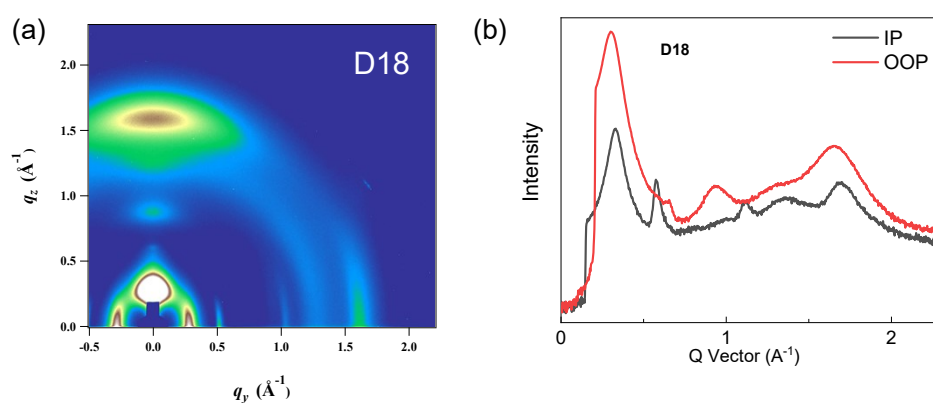


Fig. S12. (a) 2D GIWAXs images of D18 (b) corresponding 1D curves for GIWAXs of pure D18.

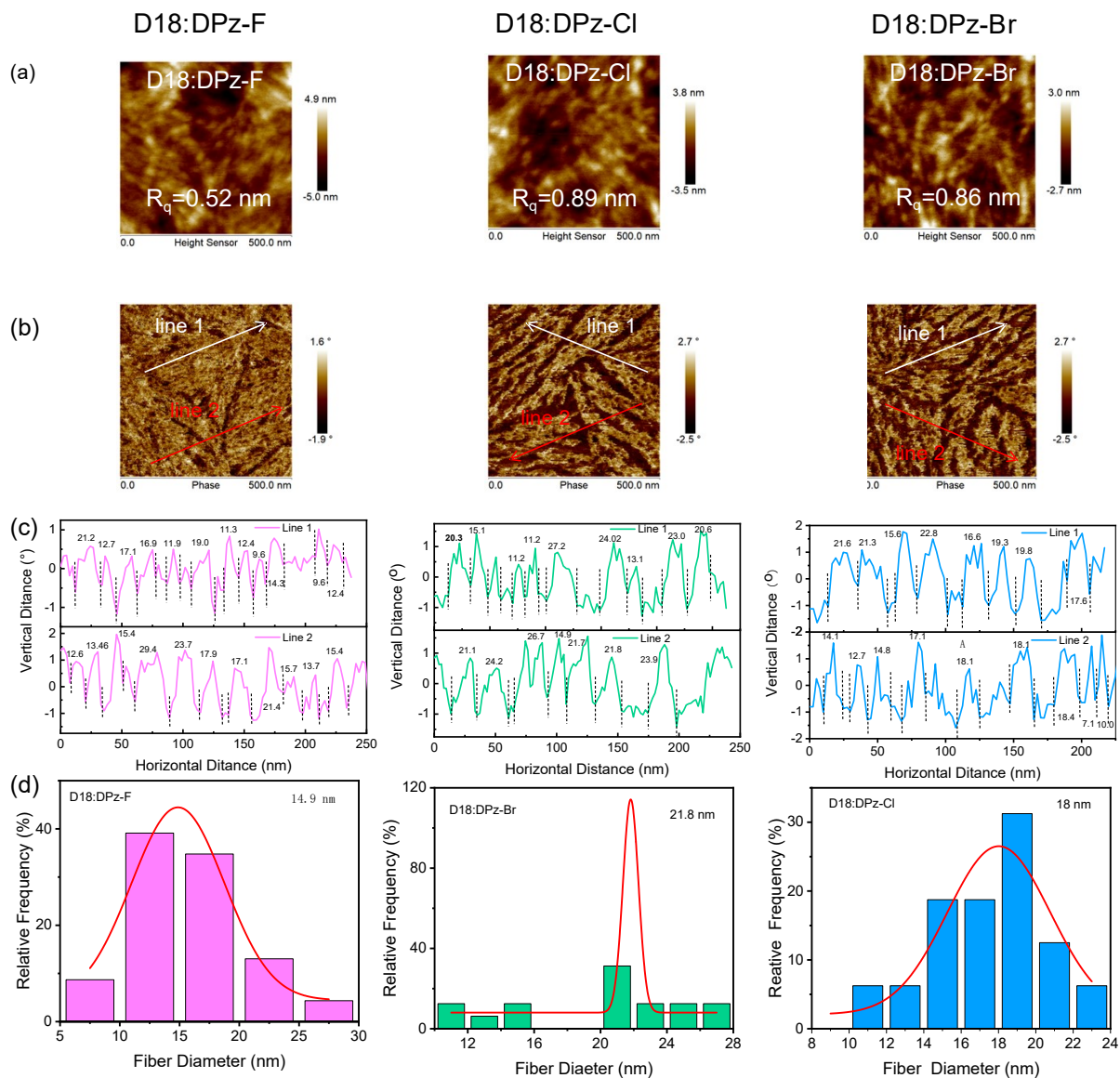


Fig. S13. (a)AFM height, (b) phase images. (c) Line profiles of the peak widths of the fiber cross-sections were obtained from the AFM phase images.(d) the statistical distribution of the fibril width for D18:DPz-F, D18:DPz-Cl and D18:DPz-Br based blended films.

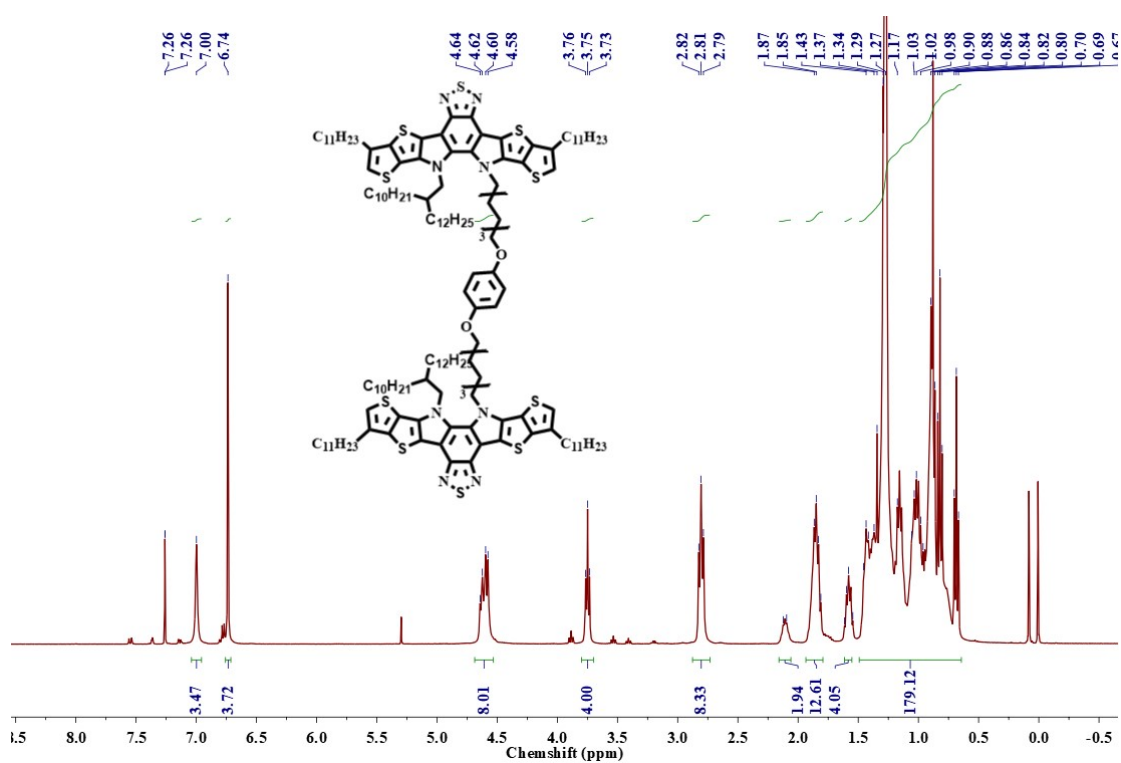


Fig.S14. ^1H NMR spectrum of compound 2 (CDCl_3).

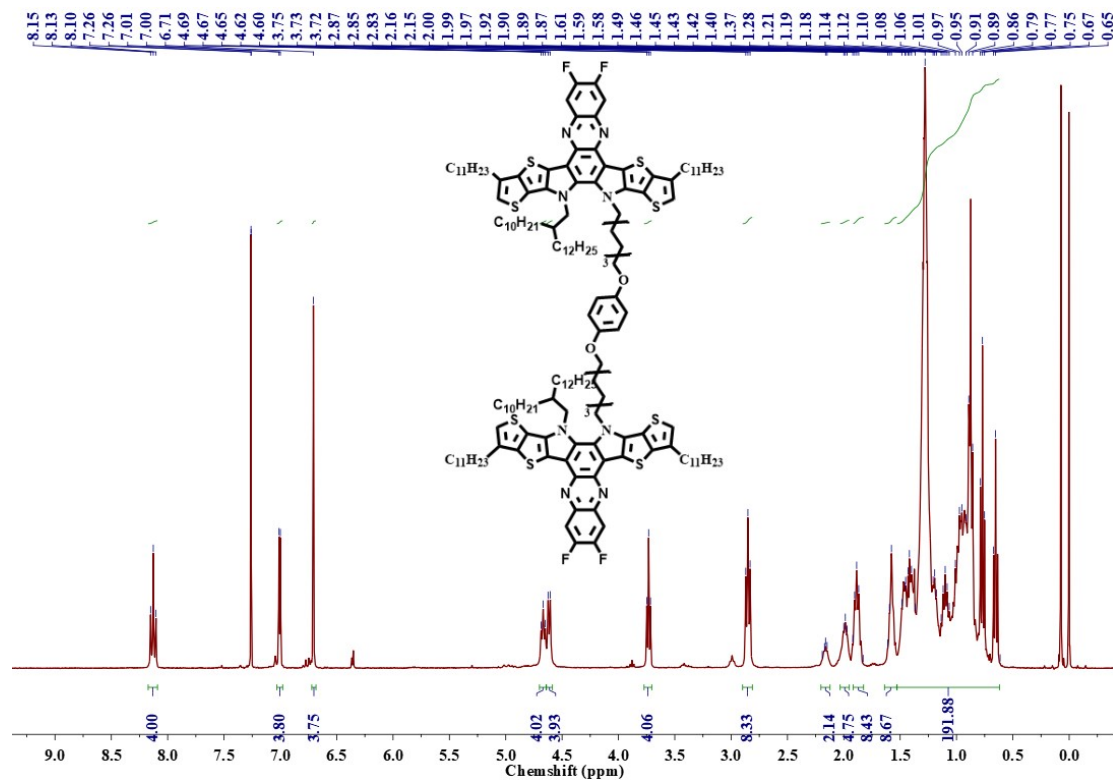


Fig.S15. ^1H NMR spectrum of compound 3a (CDCl_3).

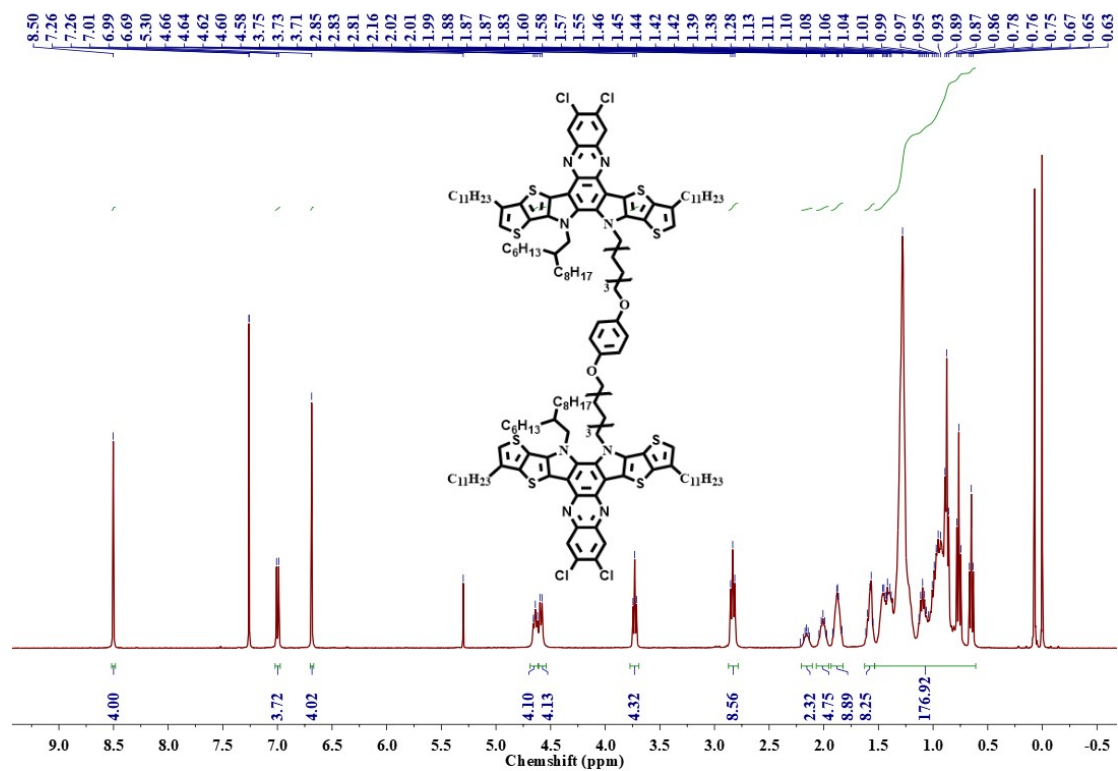


Fig.S16. ¹H NMR spectrum of compound 3b (CDCl₃).

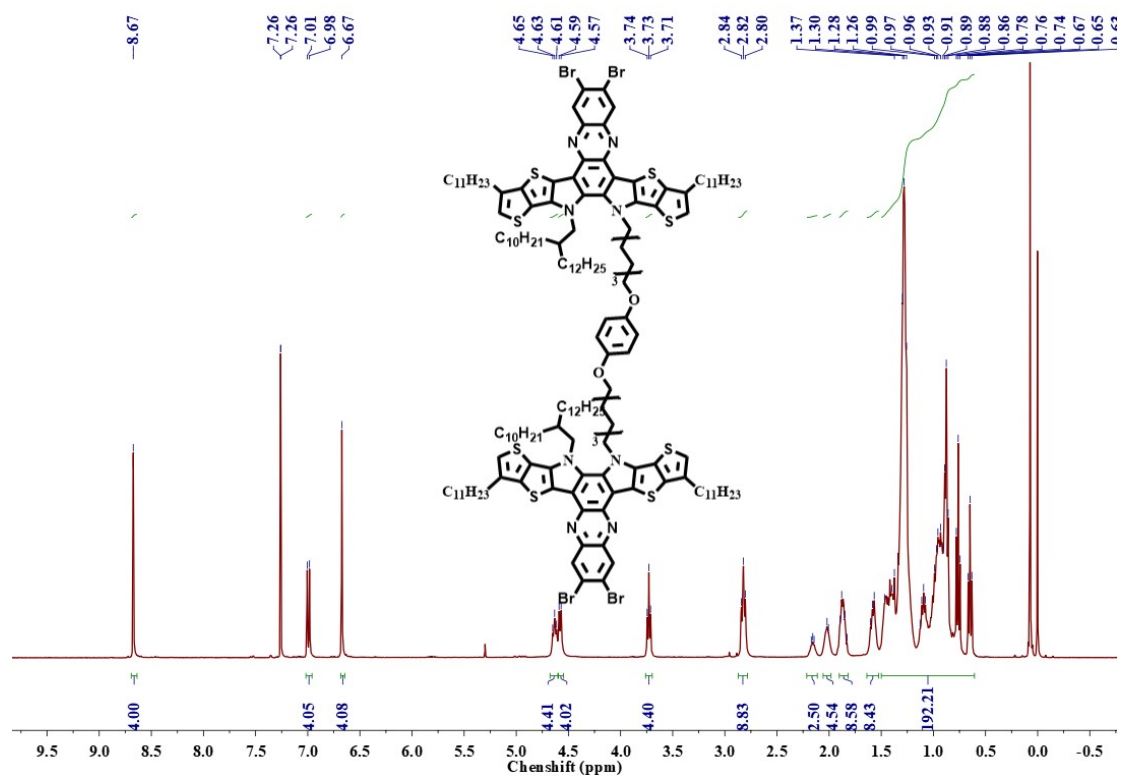


Fig.S17. ¹H NMR spectrum of compound 3c (CDCl₃).

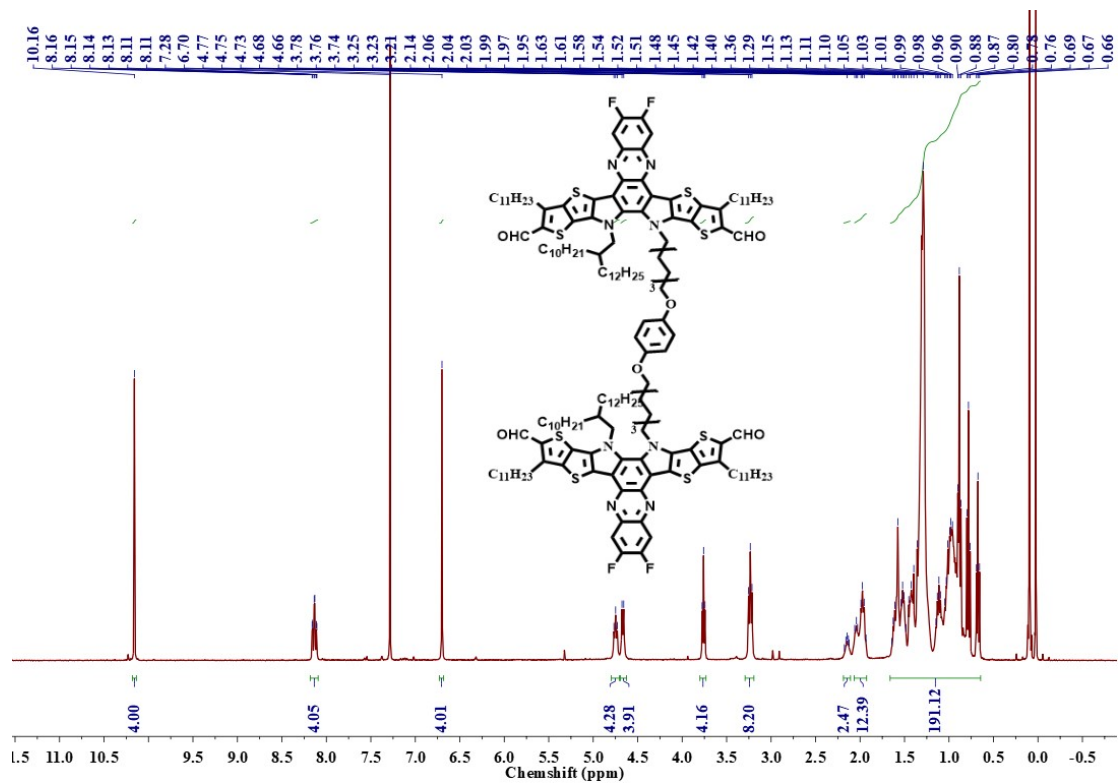


Fig.S18. ^1H NMR spectrum of compound 4a (CDCl_3).

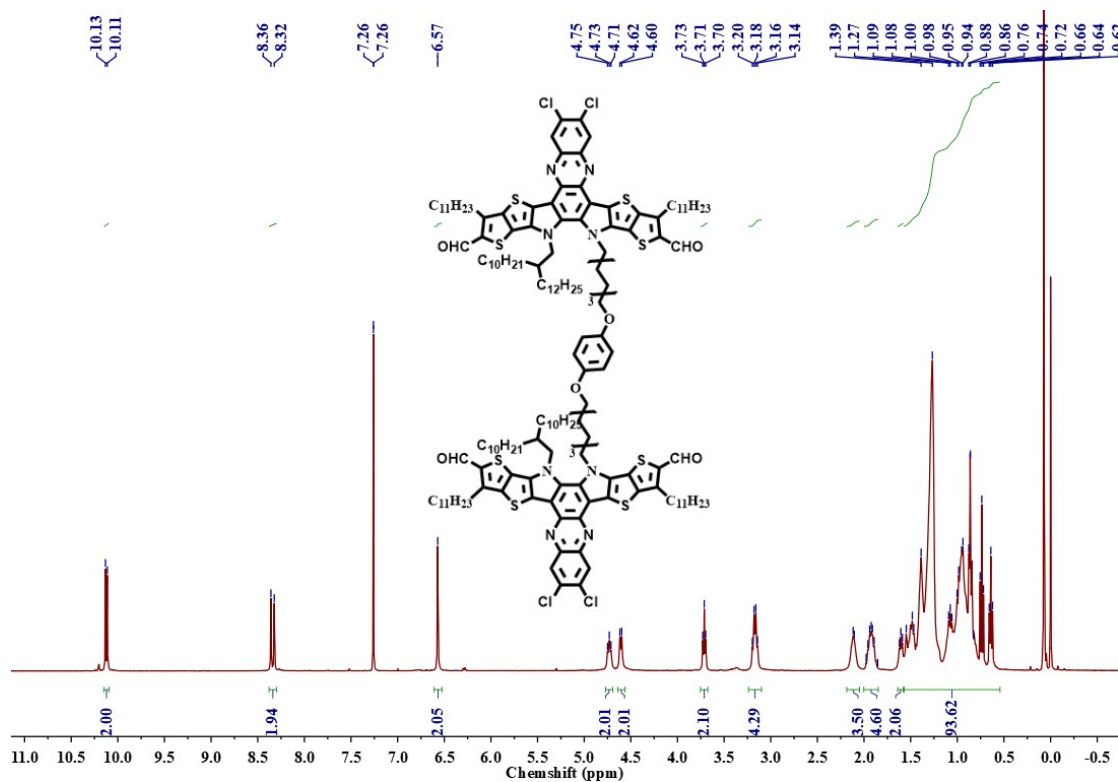


Fig.S19. ^1H NMR spectrum of compound 4b (CDCl_3).

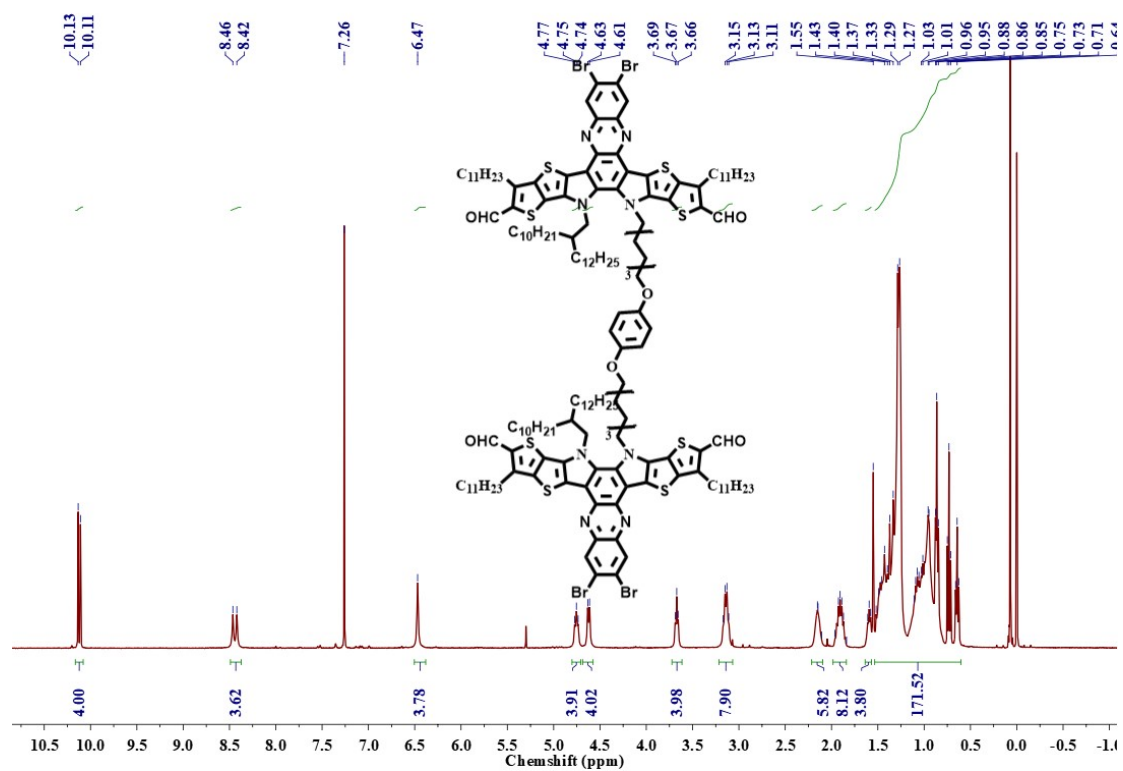


Fig.S20. ^1H NMR spectrum of **compound 4c** (CDCl_3).

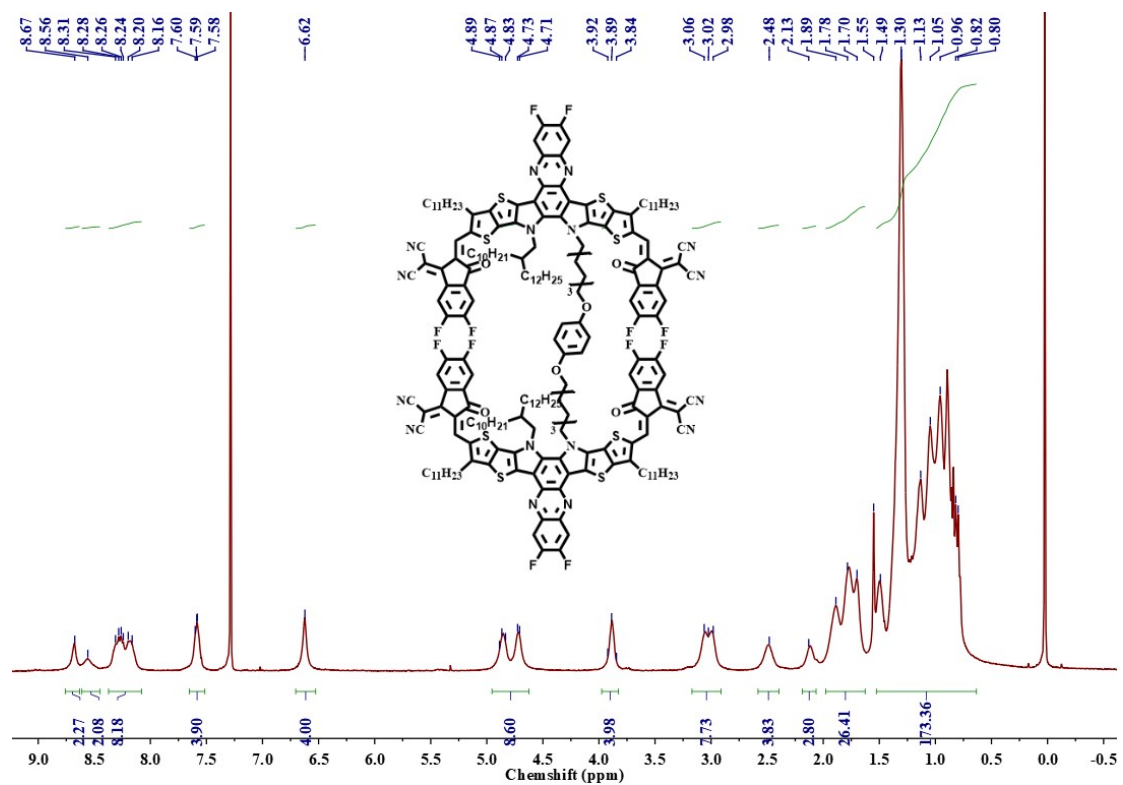


Fig.S21. ^1H NMR spectrum of DPz-F (CDCl_3).

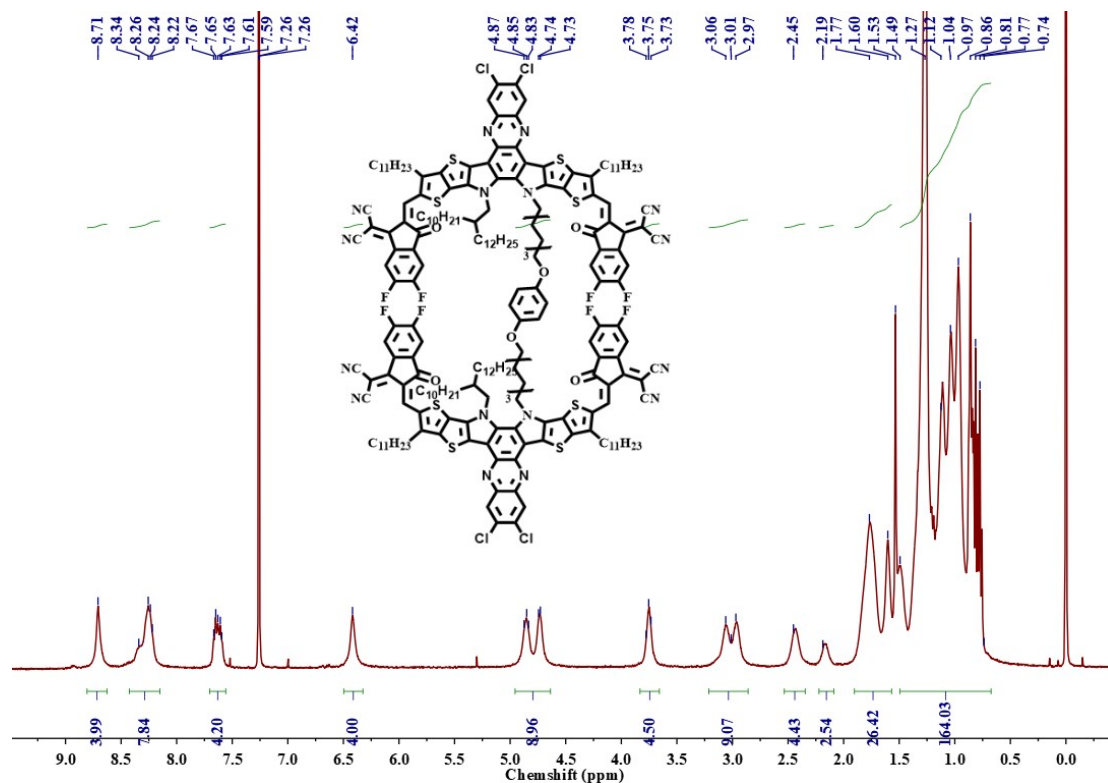


Fig.S22. ^1H NMR spectrum of DPz-Cl (CDCl_3).

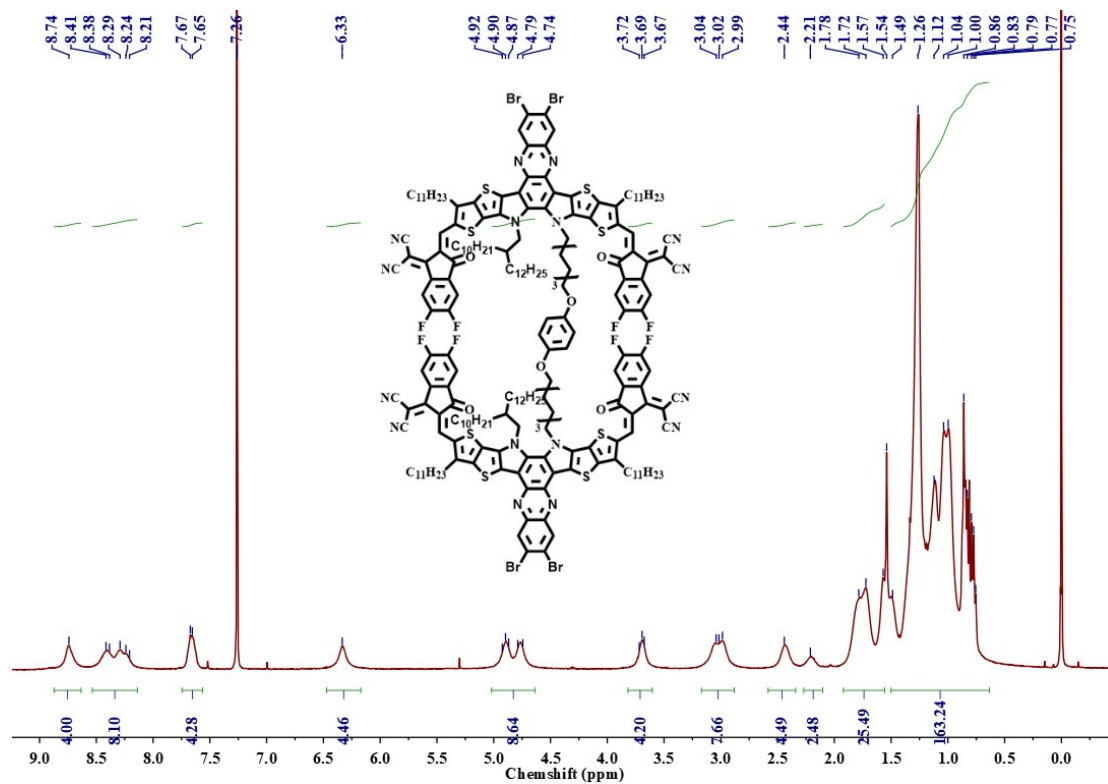


Fig.S23. ^1H NMR spectrum of DPz-Br (CDCl_3).

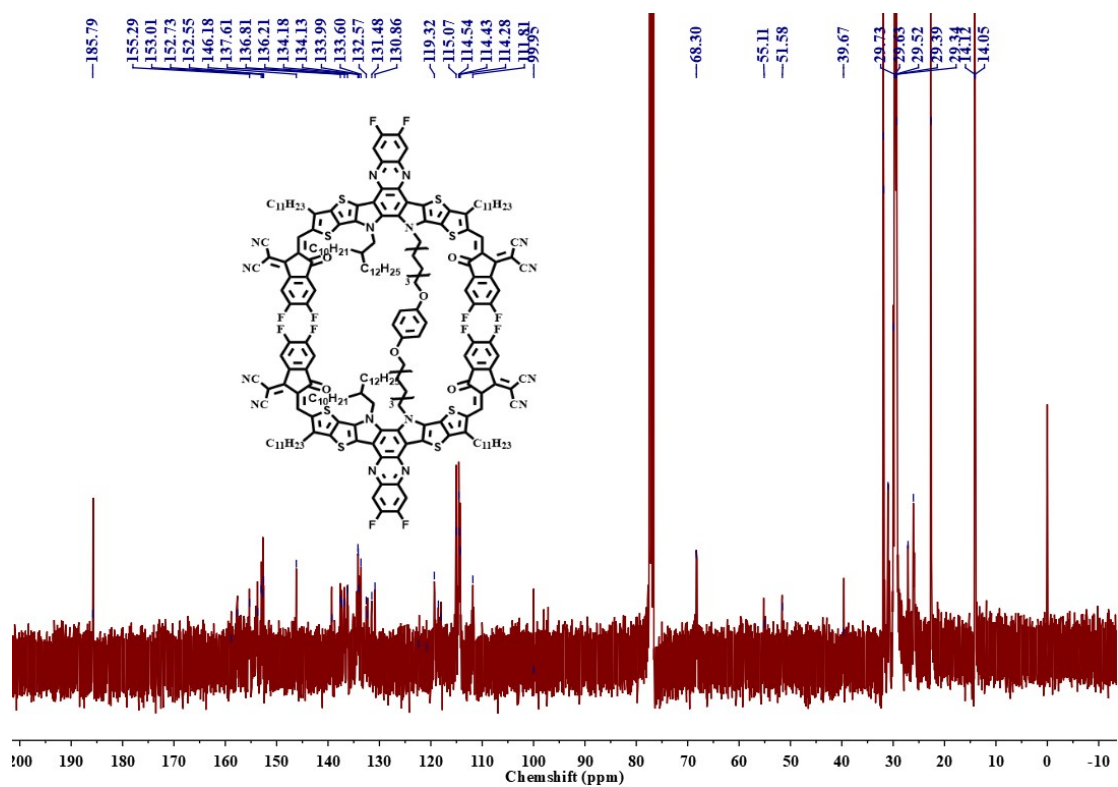


Fig.S24. ¹³C NMR spectrum of DPz-F (CDCl₃).

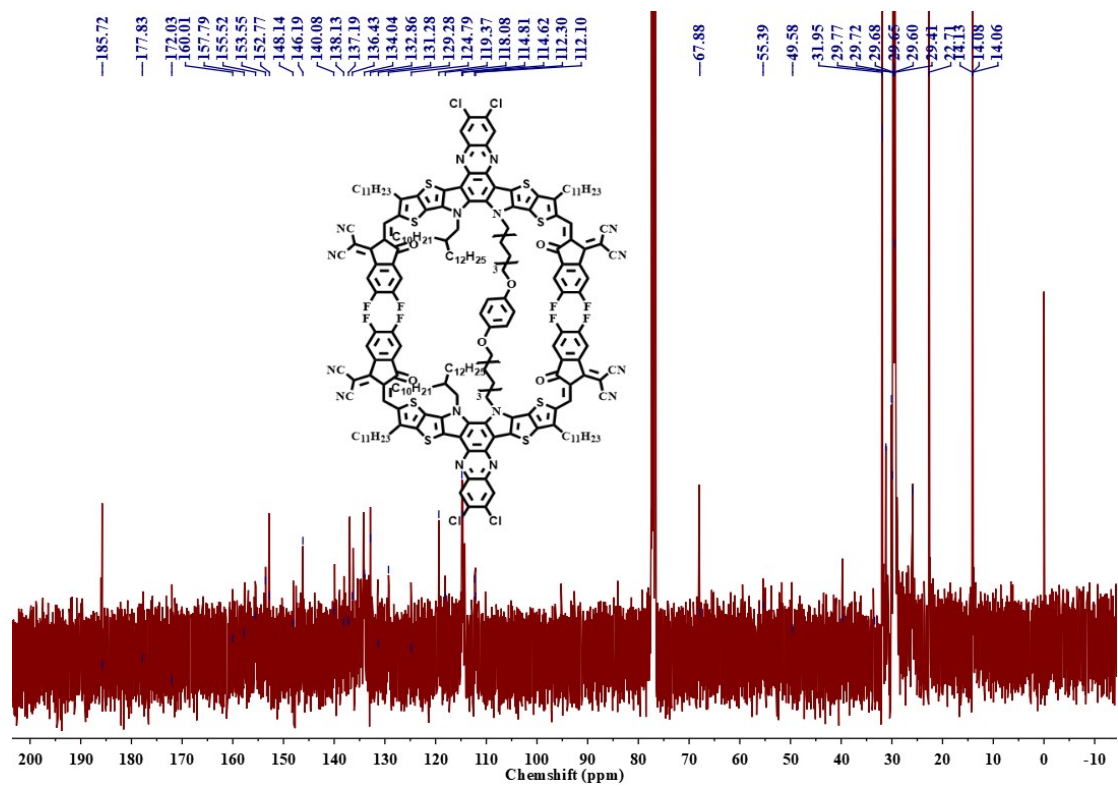


Fig.S25. ¹³C NMR spectrum of DPz-Cl (CDCl₃).

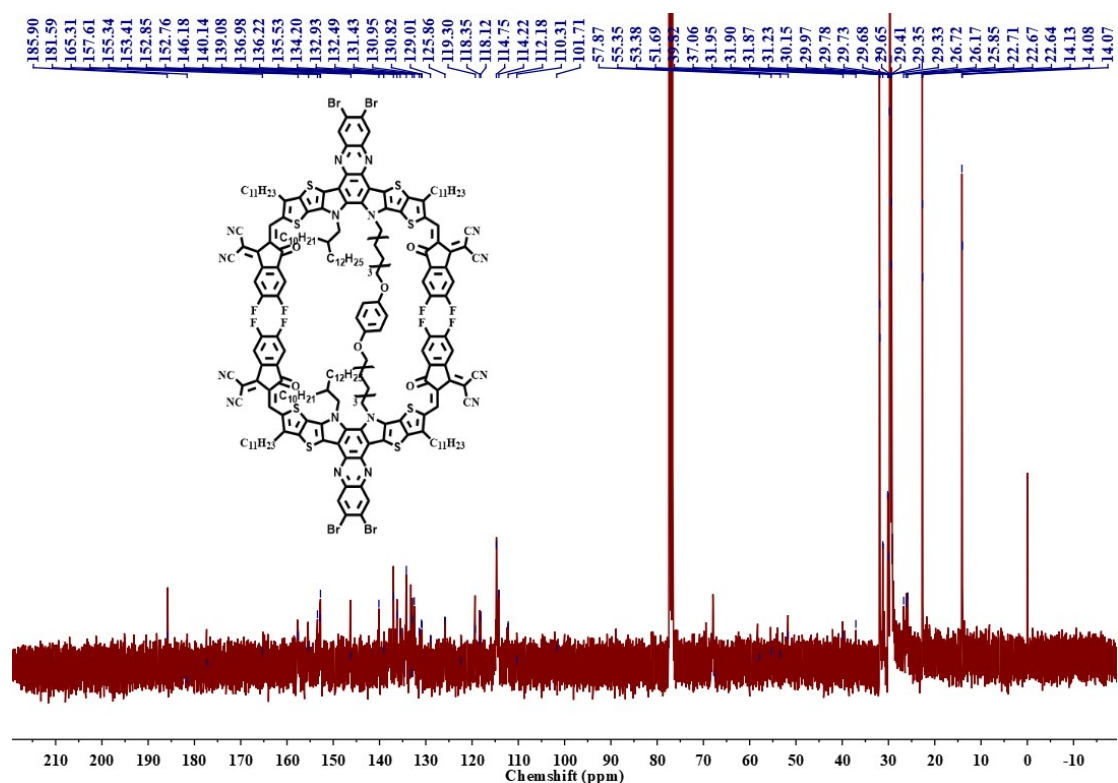


Fig.S26. ¹³C NMR spectrum of DPz-Cl (CDCl₃).

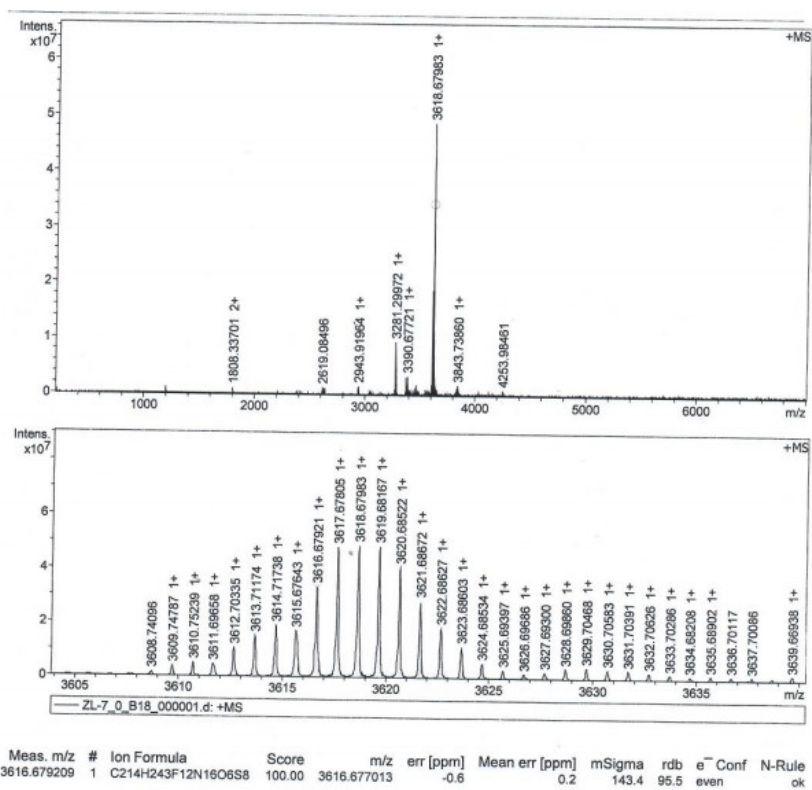


Fig.S27. MALDI-TOF MS spectrum of DPz-F

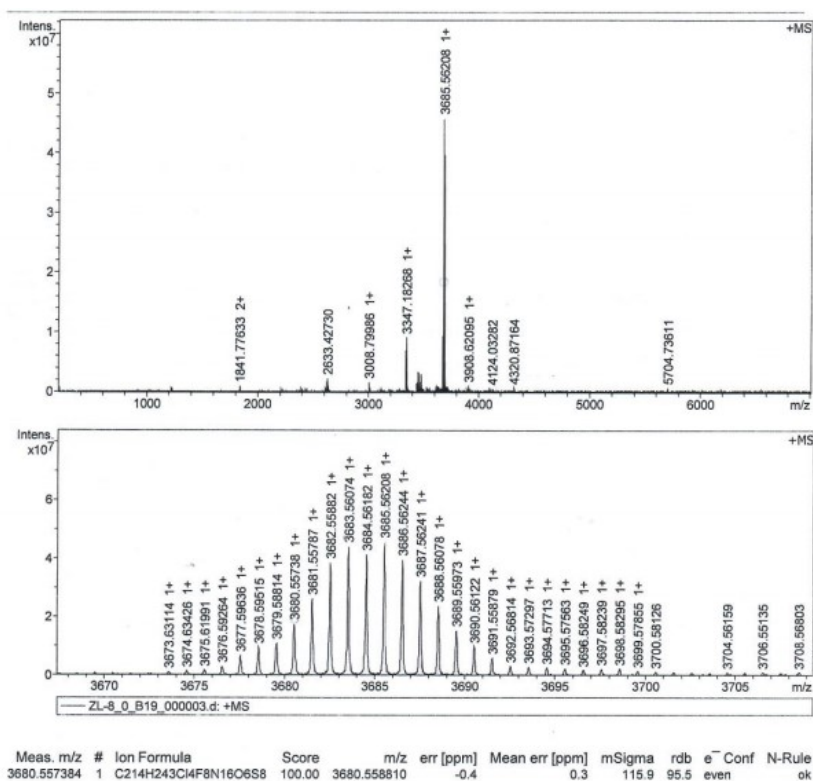


Fig.S28. MALDI-TOF MS spectrum of DPz-Cl

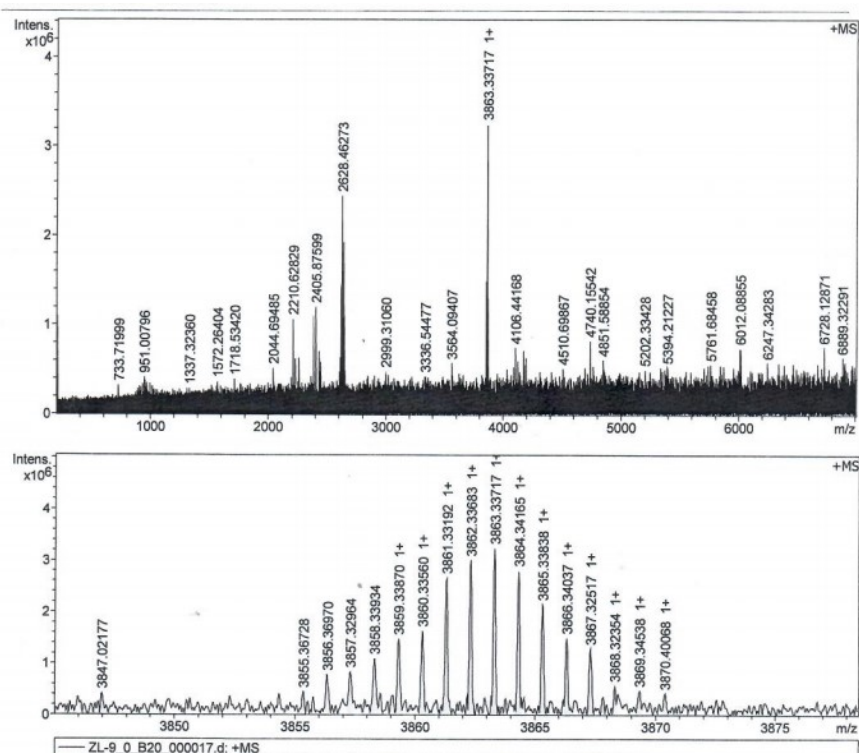


Fig.S29. MALDI-TOF MS spectrum of DPz-Br